AIAA 2003-3590

Comparison of Methods for Determining Boundary Layer Edge Conditions for Transition Correlations

Derek S. Liechty, Scott A. Berry, Brian R. Hollis,
and Thomas J. Horvath

NASA Langley Research Center
Hampton, VA 23681

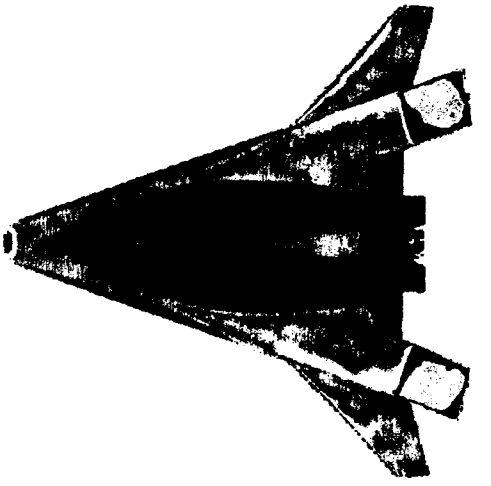

33rd AIAA Fluid Dynamics Conference and Exhibit
June 23-26, 2003
Orlando, Florida

COMPARISON OF METHODS FOR DETERMINING BOUNDARY LAYER EDGE CONDITIONS FOR TRANSITION CORRELATIONS

Derek S. Liechty*, Scott A. Berry*, Brian R. Hollis†, Thomas J. Horvath*
NASA Langley Research Center
Hampton, VA 23681

ABSTRACT

Data previously obtained for the X-33 in the NASA Langley Research Center 20-Inch Mach 6 Air Tunnel have been reanalyzed to compare methods for determining boundary layer edge conditions for use in transition correlations. The experimental results were previously obtained utilizing the phosphor thermography technique to monitor the status of the boundary layer downstream of discrete roughness elements via global heat transfer images of the X-33 windward surface. A boundary layer transition correlation was previously developed for this data set using boundary layer edge conditions calculated using an inviscid/integral boundary layer approach. An algorithm was written in the present study to extract boundary layer edge quantities from higher fidelity viscous computational fluid dynamic solutions to develop transition correlations that account for viscous effects on vehicles of arbitrary complexity. The boundary layer transition correlation developed for the X-33 from the viscous solutions are compared to the previous boundary layer transition correlations. It is shown that the boundary layer edge conditions calculated using an inviscid/integral boundary layer approach are significantly different than those extracted from viscous computational fluid dynamic solutions. The present results demonstrate the differences obtained in correlating transition data using different computational methods.

NOMENCLATURE

h	heat transfer coefficient, $h=q/(H_{aw}-H_w)$, ($kg/m^2/s$)
H	enthalpy (J/kg)
k	roughness element height (mm)
L	length of vehicle from nose to end of engine module (m)
M	Mach number
q	surface heat transfer rate (W/cm^2)
Re	unit Reynolds number (1/m)
Re_θ	momentum thickness Reynolds number, $Re_\theta = \frac{\rho_e U_e \theta}{\mu_e}$
T	temperature (K)
U	velocity magnitude (m/s)
α	angle-of-attack (deg)
δ	boundary layer thickness (mm)
θ	momentum thickness (mm) $\theta = \int_0^\delta \left(\frac{\rho U}{\rho_e U_e}\right)\left(1-\frac{U}{U_e}\right)$
μ	viscosity (kg/m/s)
ρ	density (kg/m^3)

Subscripts

∞	freestream static conditions
aw	adiabatic wall conditions
e	local edge conditions
FR	conditions from Fay-Riddell calculation for a hemisphere
w	model surface conditions
tr	transition onset
inc	incipient
eff	effective

INTRODUCTION

The ability to accurately predict when boundary layer transition will occur on a flight vehicle is important when considering the sizing of a thermal protection system (TPS). In recent studies[1,2], transition correlations were generated for a set of wind tunnel data using boundary layer edge conditions calculated using inviscid/integral boundary layer techniques. However, it is now reasonable to generate transition correlations for arbitrarily complex vehicle geometries using boundary layer edge conditions extracted from higher fidelity viscous CFD solutions. This approach was used in a recent Mars Science Lander transition study[3] and has been applied to the X-33 experimental aeroheating database in the present study.

* Aerospace Technologist
† Aerospace Technologist, Senior Member AIAA

Berry[1] has recently addressed the importance of the computational method used when generating transition correlations. Different computational methods can provide significant differences in the calculated edge properties used to form the correlations, as noted in Refs. 4 and 5, and the use of a correlation must be consistent with the computational method used. Therefore, the purpose of the present study is to compare previous correlations made using an inviscid/approximate boundary layer code to correlations generated using boundary layer edge quantities extracted from viscous CFD solutions.

The X-33 vehicle, which was intended to be a sub-orbital, half-scale representation of a Single-Stage-to-Orbit Reusable Launch Vehicle (SSTO-RLV)[2,6-8], was selected as the basis for this study. Although the program is no longer active, a large experimental/computational aerothermodynamic database[9-17] was developed by NASA for the X-33, and a considerable investment was made to produce computational surface geometries and grids and to design and fabricate wind tunnel models. Therefore, the X-33 configuration was an ideal choice for this study.

The present study utilized the same discrete roughness transition correlation methodologies used during investigations into discrete roughness elements on Shuttle Orbiter[1,18], X-33[11], and X-38[19]. These studies have used the transition parameter Re_θ/M_e (the momentum thickness Reynolds number divided by the local edge Mach number) along with the boundary layer thickness, discrete roughness height, and experimental transition results to correlate the data.

X-33 VEHICLE GEOMETRY

The computational results presented in this reference are based on the 604B002F configuration of the Lockheed-Martin X-33 vehicle, which is commonly referred to as the F-Loft, Rev-F configuration. This configuration (Fig. 1) is a lifting-body delta planform with twin vertical tails, canted fins and body flaps. The body length is 19.3 m (63.2 ft.) from the nose to the end of the engine module, and the span across the canted fins is 23.2 m (76.1 ft.). The canted fins have a dihedral of 20-deg and a -8.58-deg incidence angle.

EXPERIMENTAL RESULTS

The results presented in Ref. 11, from Test 6770 in the NASA Langley 20-Inch Mach 6 Air Tunnel, were reanalyzed in order to formulate new transition correlations based on higher fidelity viscous CFD solutions in the present study. Representative flow conditions for each of the standard 20-Inch Mach 6 Air Tunnel operating points at which tests were conducted have been computed using the GASPROPS[20] code and are listed in Table 1. The flow conditions listed in Table 1 were used as the free stream flow conditions used in the viscous CFD solutions from which boundary layer edge conditions were extracted in the present study at angles-of-attack of 20-degrees, 30-degrees, and 40-degrees.

Global surface heating distributions were obtained using the digital optical measurement method of two-color, relative-intensity, phosphor thermography[21-25]. The heating data are presented herein in terms of a non-dimensional heat transfer

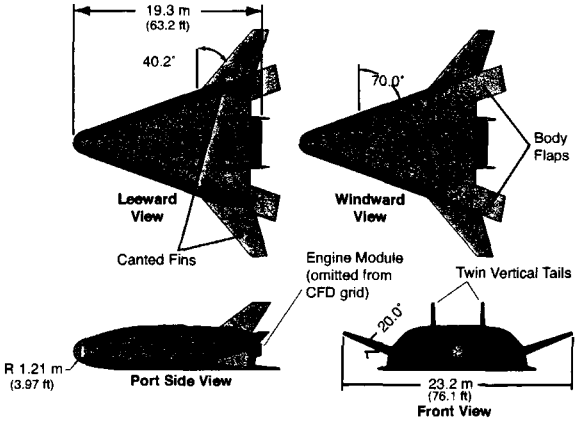

Figure 1: Dimensioned Sketch of Full-Scale X-33 F-Loft, Rev-F Configuration.

Operating Condition	Re_∞/ft	M_∞	T_∞ (K)	ρ_∞ (kg/m^3)	U_∞ (m/s)	h_{FR} (kg/m^2/s)	q_{FR} (W/cm^2)
$Re_\infty = 9.46\text{x}10^6$/m	$2.88\text{x}10^6$	6.00	62.099	$4.4511\text{x}10^{-2}$	946.61	0.45806	9.5938
$Re_\infty = 13.13\text{x}10^6$/m	$4.00\text{x}10^6$	6.00	62.325	$6.1947\text{x}10^{-2}$	947.73	0.54117	11.403
$Re_\infty = 15.29\text{x}10^6$/m	$4.66\text{x}10^6$	6.01	63.240	$7.2564\text{x}10^{-2}$	956.12	0.59208	13.004

Table 1: Wind Tunnel Free Stream Conditions

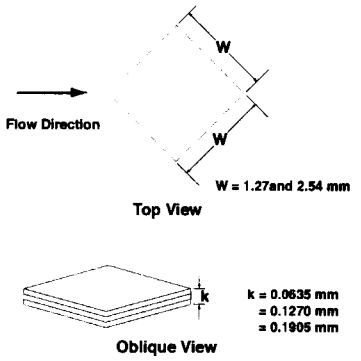

Figure 2: Trip Sketch Showing Orientation, Width, and Height.

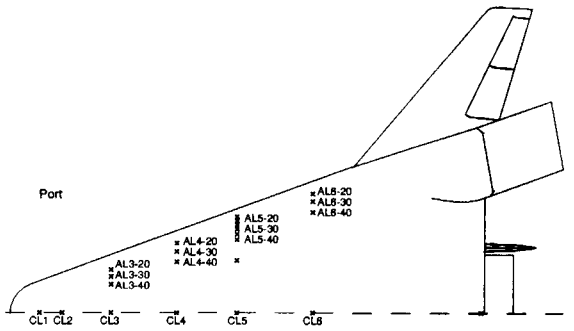

Figure 3: Trip Locations and Fiducial Marks.

coefficient ratio, h/h_{FR}, where h_{FR} is the theoretical heating computed with the Fay-Riddell[26] method for a sphere of the radius of the nose of the test models, with a wall temperature of 300 K.

The cast ceramic aeroheating models were 0.0132-scale representations of the full scale vehicle, resulting in a 0.254 m (10.0-in.) model length measured from the nose to the end of the engine module. Discrete roughness elements were produced by application of 0.064 mm to 0.1905 mm (0.0025-in. to 0.0075-in.) height squares of polyimide film with a silicone adhesive. Roughness elements (Fig. 2) fabricated from the film were applied to the various locations of interest on the model and could be easily removed without adversely affecting the phosphor coating. The roughness elements were placed directly over the various fiducial marks both on the center-line and on the attachment lines (Fig. 3; see Ref. 11 for a complete description of test models and discrete trips and their placement).

COMPUTATIONAL METHOD

Numerical Algorithms

A boundary layer transition correlation for X-33 was previously developed[2] using the engineering code LATCH (Langley Approximate Three-Dimensional Convective Heating)[27] to obtain the boundary layer edge properties. The LATCH code is an approximate three-dimensional heating code based on the axisymmetric analog for general three-dimensional boundary layers. An integral heating method is used to compute the heating rates along three-dimensional inviscid streamlines. The inviscid streamlines were supplied by the LAURA (Langley Aerothermodynamic Upwind Relaxation Algorithm)[28,29] code run in an inviscid mode. The LAURA code is a three-dimensional, finite-volume fluid dynamics solver for steady-state flows. Roe-averaging (Ref. 30) with Harten's entropy fix (Ref. 31) and Yee's Symmetric Total Variation Diminishing limiter (Ref. 32) is used for inviscid fluxes, and a second-order scheme is employed for viscous fluxes. Further details regarding the LATCH computations can be found in Ref. 10.

For the current study, laminar, perfect-gas air aeroheating computations were performed at the wind tunnel test conditions using the thin-layer Navier-Stokes LAURA option. Free stream conditions for the computations were set to the nominal operating conditions of the NASA LaRC 20-Inch Mach 6 Air Tunnel, which are listed in Table 1. For these computations, a uniform, ambient 300 K wall temperature boundary condition was imposed. The use of a constant wall temperature was valid because the experimental data were reported in terms of the non-dimensional ratio, h/h_{FR}, which is approximately constant with wall temperature. The computational grid used in Ref. 12 was utilized in the present study (see Fig. 4). This grid, which was originally used in

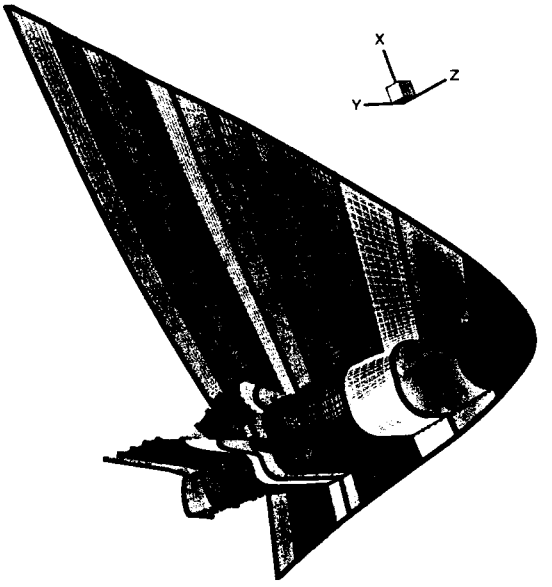

Figure 4: Bow shock aligned computational grid for vehicle at $\alpha = 30$-degrees.

the GASP[33] CFD solver, contained approximately 1.73 million grid points. The grid was decomposed into 16 computational blocks and was adapted to align the grid with the bow shock and cluster grid points in the boundary layer with a wall cell Reynolds number of approximately 3.

A comparison of windward centerline heating distributions between computations using LAURA and experiment at α = 20-degrees, 30-degrees, and 40-degrees is shown in Figure 5. The experimental data, which are taken from Ref. 11, show an increase in heating near the aft region of the model as the free stream Reynolds number was increased. This is due to the onset of natural transition. The laminar computational predictions generally agree within ±10% of the laminar experimental data at all values of Re_∞ (there is no Reynolds number effect on non-dimensional laminar heating).

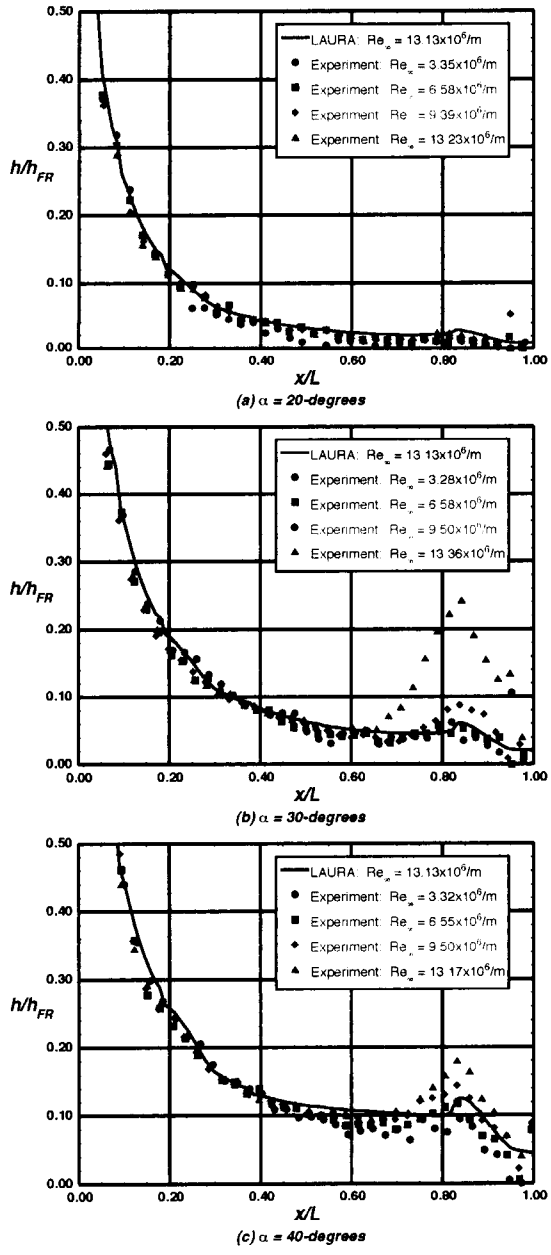

Figure 5: Comparison of Measured (see Ref. 11) and Predicted Values of Centerline Heating.

Boundary Layer Edge Definition

Engineering relations[34] are used within LATCH to obtain both the momentum thickness *(θ)* and the boundary layer thickness *(δ)*, where θ is calculated based on local properties and δ is determined based on the shape factor relation of δ/θ = 5.5. The boundary layer edge properties are obtained by interpolating in the inviscid flowfield a distance equal to the boundary layer thickness away from the wall. To accomplish this, an initial assumption is made for the boundary layer edge properties (usually the wall values), and the boundary layer thickness is computed. Then the edge properties are re-computed based on this new location within the flowfield and the solution is iterated until the re-computed boundary layer thickness is equal to the assumed value. This process usually takes two or three iterations to converge. The use of edge properties determined in this manner approximately accounts for the effect of variable entropy at the boundary layer edge. Recent experience with moderately blunt bodies like the Orbiter, however, has shown that based on the inviscid solutions available, iterating away from the surface has a minimal affect on the convective heating solutions (the primary motivation for the code), even though it provides for more exact edge conditions. By assuming the boundary layer edge properties to be equal to the inviscid surface conditions, which corresponds to a constant entropy condition, solutions are obtained much more quickly. Since the correlations previously formed for the X-33 were based on a constant entropy assumption, the boundary layer edge conditions from the inviscid/integral results presented herein are actually the inviscid wall conditions.

In order to extract boundary layer edge conditions from the LAURA solutions, a post-processing algorithm was written. This algorithm computes surface normals at each computational point on the surface of the model and iterates along the normal until the boundary layer edge is found, which is defined as a specified value of the ratio $H_0/H_{0,\infty}$ (discussed later). Once the edge is found, flow properties are interpolated at discrete points along the surface normal in order to extract the boundary layer profile. The

momentum thickness can then be calculated by integrating over the boundary layer.

The criteria for which the edge of the boundary layer is defined can change throughout the speed regime from subsonic through hypersonic. For many flows, the boundary layer edge is defined where the velocity is equal to 99% of the free stream velocity. However, this assumption is not always valid for hypersonic flows, where viscous effects can be much more significant. The criterion most often used to define the boundary layer edge in hypersonic flows is the location along the wall normal at which the local stagnation enthalpy (H_0) is equal to 99.5% of the free stream stagnation enthalpy. This definition can be used because, for an inviscid, adiabatic steady flow with no body forces, the total enthalpy is constant along a given streamline. Thus, outside of the boundary layer, the stagnation enthalpy should be constant.

BOUNDARY LAYER EDGE PROPERTIES COMPARISON

Sensitivity to Boundary Layer Edge Definition

The sensitivity of the boundary layer thickness, momentum thickness Reynolds number, and edge Mach number with respect to the definition of the fraction of the local stagnation enthalpy to the free stream stagnation enthalpy are shown in Figures 6, 7, and 8, respectively. Data are shown along the windward centerline at angles-of-attack of 20-degrees, 30-degrees, and 40-degrees and a fixed free stream Reynolds number of 13.13×10^6/m. Total enthalpy ratios of $H_0/H_{0,\infty}$ = 0.950, 0.990, and 0.995 are presented from the post-processed LAURA solutions. The $H_0/H_{0,\infty}$ = 0.950 boundary layer height, momentum thickness Reynolds number, and edge Mach number calculations were approximately 20%, 30%, and 10% lower than the $H_0/H_{0,\infty}$ = 0.990 calculations, respectively. The difference between the $H_0/H_{0,\infty}$ = 0.990 and 0.995 calculations is below 5% for the three boundary layer properties considered. This suggests that defining the boundary layer edge as the location where the stagnation enthalpy ratio is $H_0/H_{0,\infty}$ = 0.995 is appropriate.

Comparison of Method of Calculation

Comparisons of boundary layer edge parameters along the windward centerline between LATCH solutions and the post-processed LAURA solutions are also shown in Figures 6-8. The windward centerline boundary layer height, δ, is presented in Figure 6. For all angles-of-attack, δ at the nose is comparable between the LATCH and post-processed LAURA solutions. However, as the running length increases, the boundary layer height extracted from LAURA increased at a greater rate than the LATCH solutions. This trend decreased as angle-of-attack was increased. Therefore, it appears that the LATCH solution was under-predicting the boundary layer height, especially at α = 20-degrees. This greater difference at 20-degrees may be due to the thickening of the

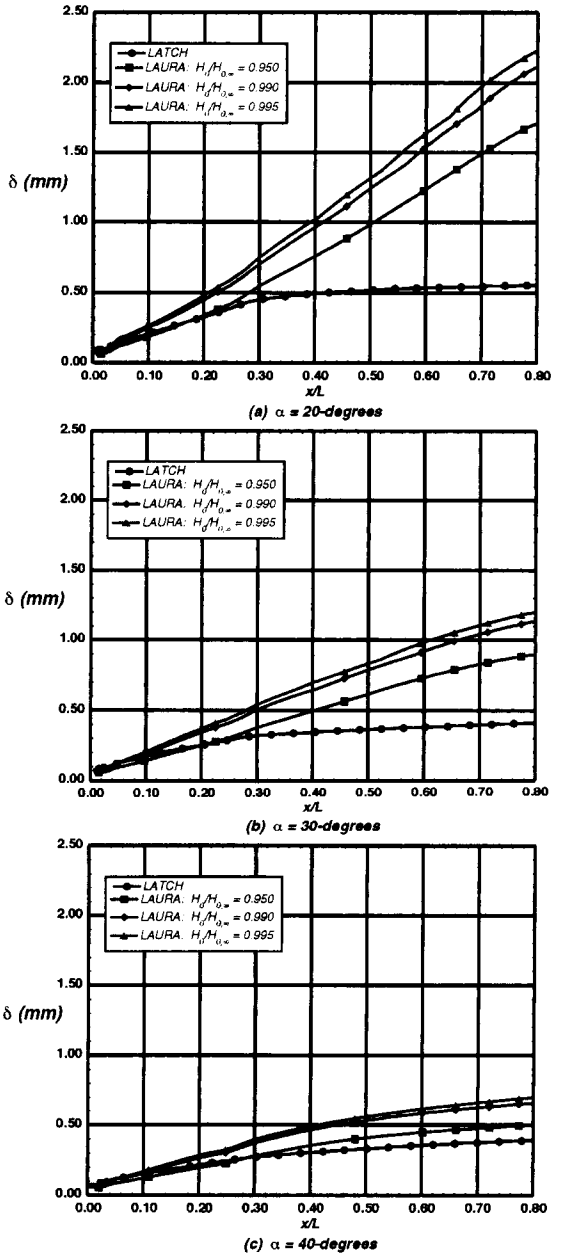

Figure 6: Boundary Layer Thickness as Calculated from LAURA at Varying Stagnation Enthalpy Ratios and from LATCH at Re_∞ = 13.13×10^6/m.

boundary layer along the centerline due to inflow from the attachment lines[11].

For Re_θ (Figure 7), the LAURA and LATCH solutions compared favorably up to approximately x/L = 0.25, but the solutions diverged downstream of this point, with the LAURA solution predicting a higher value of Re_θ. Once again, the difference between the two solutions became greater as angle-of-attack was decreased.

The divergence of the computed values of edge Mach number (Figure 8), however, was in the opposite direction. The post-processed LAURA solutions predict a value of M_e which was lower than that of the LATCH solution. The edge Mach number calculated by post-processing the LAURA solution was approximately 20% lower than that calculated by LATCH.

When comparing methods of calculating boundary layer edge conditions using inviscid/engineering methods, Berry[1] showed that when the boundary layer

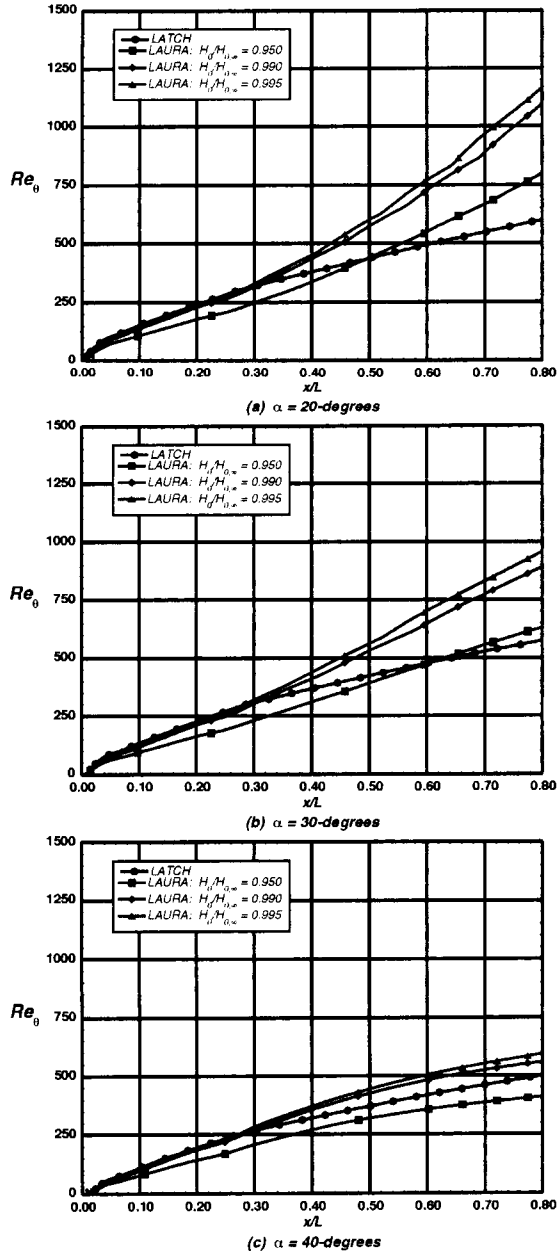

Figure 7: Momentum Thickness Reynolds Number as Calculated from LAURA at Varying Stagnation Enthalpy Ratios and from LATCH at Re_∞ = 13.13x10^6/m.

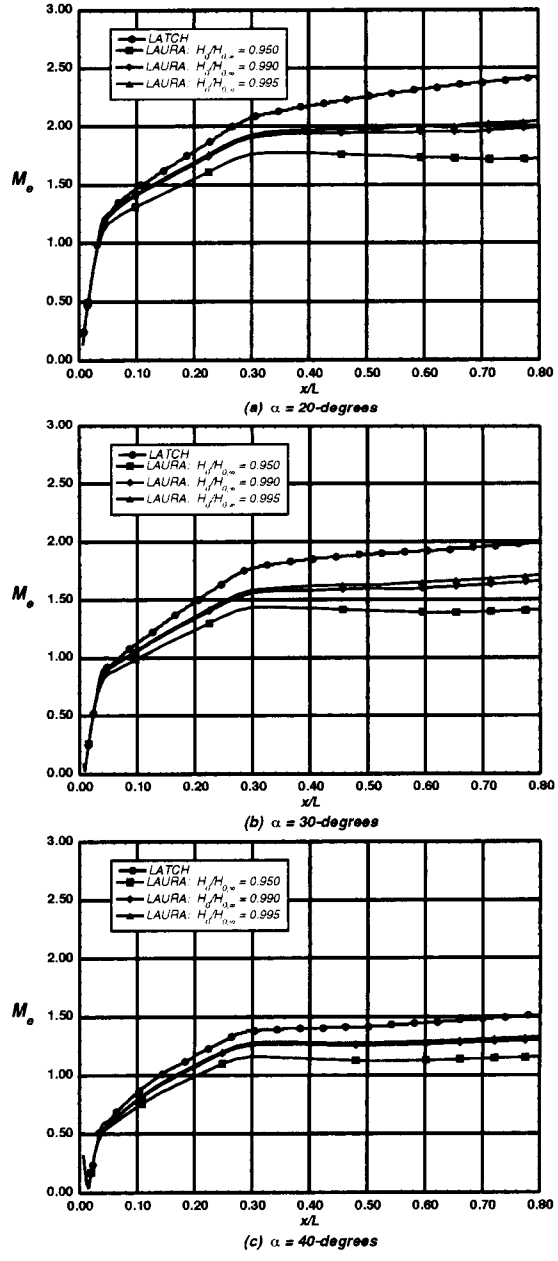

Figure 8: Edge Mach Number as Calculated from LAURA at Varying Stagnation Enthalpy Ratios and from LATCH at Re_∞ = 13.13x10^6/m.

transition parameter Re_θ/M_e was examined, the methods fortuitously showed good agreement, due to the cancellation of differences in Re_θ and M_e. This parameter is shown along the windward centerline at α = 20-degrees, 30-degrees, and 40-degrees for the LATCH and post-processed LAURA ($H_0/H_{0,\infty}$ = 0.995) solutions in Figure 9. The two solutions compare well upstream of approximately x/L = 0.25.

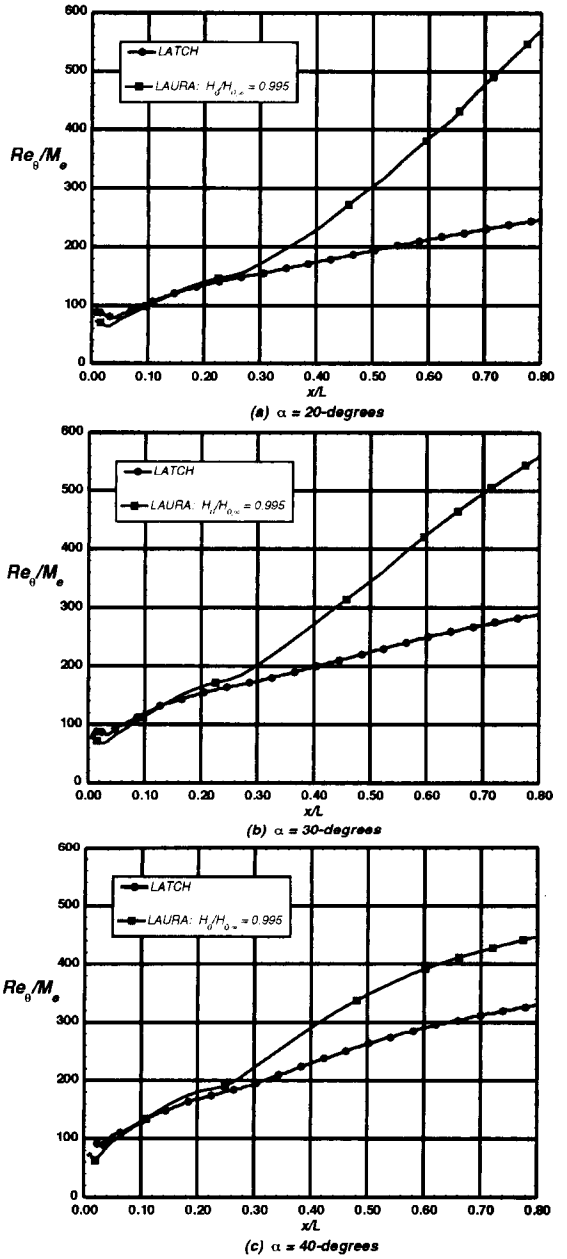

Figure 9: Re_θ/M_e as Calculated from LAURA at $H_0/H_{0,\infty}$ = 0.995 and from LATCH at Re_∞ = 13.13x10^6/m.

Downstream of x/L = 0.25, however, the transition parameter calculated by LATCH was lower than that of the post-processed LAURA solution. This difference once again became more pronounced as angle-of-attack was decreased.

BOUNDARY LAYER TRANSITION CORRELATION

The results presented in Ref. 11, from Test 6770 in the NASA Langley 20-Inch Mach 6 Air Tunnel, were used to generate a new, higher fidelity transition correlation based on boundary layer edge conditions extracted from the viscous CFD solver LAURA. Approximately 100 data points were used from this test in the current study. Data points from along the centerline and along the attachment lines were included. Laminar computations were performed using LAURA for a complete wind tunnel test range of angles-of-attack (α = 20-deg, 30-deg, and 40-deg) and a selection of Reynolds numbers (Re_∞ = 9.46x10^6/m, 13.13x10^6/m and 15.29x10^6/m) in order to determine boundary layer edge properties (Re_θ, M_e, and δ), which were used to formulate transition correlations from the experimental data.

For each discrete roughness element in each experimental run which was reanalyzed, the state of the boundary layer downstream of the element was determined through visual inspection of the surface heating images and classified as either: laminar; transition at some distance downstream of the discrete roughness element; or transition effective (i.e. immediately downstream of) from the discrete roughness element. Examples of experimental data which fit each of these classifications are shown in Fig. 10.

The results of X-33 transition correlations generated using LATCH were presented in Ref. 2. Two simple curves were suggested as laminar and turbulent boundaries (shown in Fig 11 as dashed curves). The first curve (incipient) was defined as the boundary between laminar flow downstream of the discrete roughness element and transitional flow downstream of the element. The second curve (effective) was defined as the boundary between transitional flow downstream of the element and where the transitional wedge was attached to the roughness element.

Data points taken from the experimental study where the boundary layer edge conditions were instead extracted from LAURA solutions are also shown in Fig. 11. The curves suggested in Ref. 2 generated using the LATCH edge conditions were not applicable when using the LAURA edge conditions, as evident from the discussion on boundary layer edge

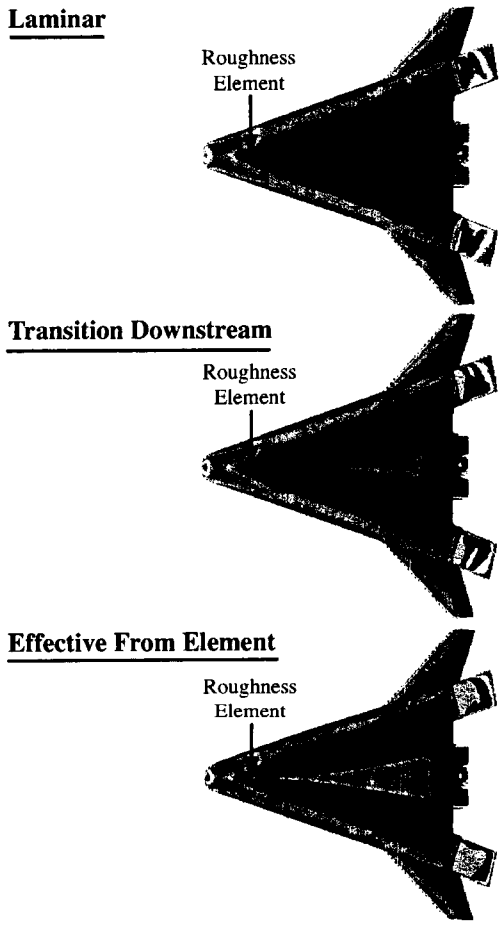

Figure 10: Classification of Discrete Roughness Effect on Boundary Layer.

properties earlier in this paper. This does not mean that the LATCH curves are incorrect. However, the present results demonstrate the differences obtained in correlating transition data using different computational methods. Based on the results of this study, two simple curves similar to those of Ref. 2, but for the LAURA boundary layer edge conditions, are suggested in Figure 11.

CONCLUSIONS

Data previously obtained for the X-33 in the NASA Langley Research Center 20-Inch Mach 6 Air Tunnel have been reanalyzed to form new boundary layer transition correlations using higher fidelity viscous computational fluid dynamic solutions. An algorithm was written in the present study to extract boundary layer edge quantities from viscous computational fluid dynamic solutions to develop transition correlations that account for viscous effects on vehicles of arbitrary complexity.

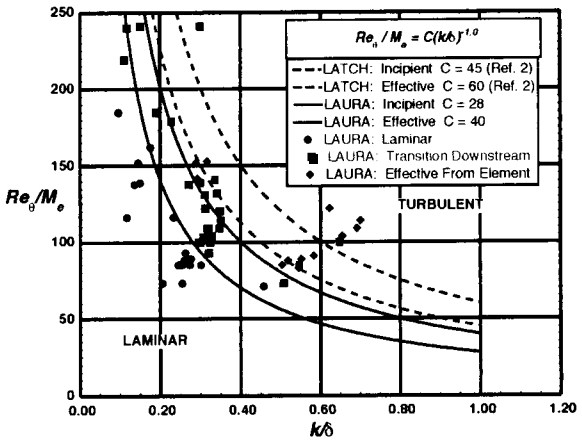

Figure 11: LATCH Transition Correlation Curves with Data Points from LAURA Solutions.

It was found that defining the boundary layer edge as the location where the ratio of local stagnation enthalpy to free stream stagnation enthalpy is equal to 0.995 was appropriate. When the LATCH and LAURA boundary layer edge quantities were compared, the boundary layer height and momentum thickness Reynolds number from LAURA were significantly higher than the inviscid/integral values; whereas the viscous edge Mach number was lower than the computed inviscid/integral value. These differences were found to increase as angle-of-attack was decreased.

When the transition correlation Re_θ/M_e vs. k/δ was revisited using the boundary layer edge quantities extracted from LAURA solutions corresponding to wind tunnel conditions, a different set of transition curves were required. This does not imply that the correlation generated using the LATCH boundary layer edge quantities was incorrect, only that when one method is used to obtain boundary layer edge conditions, the corresponding set of curves must be used.

REFERENCES

[1]Berry, S. A., and Hamilton II, H. H., "Discrete Roughness Effects on Shuttle Orbiter at Mach 6," AIAA Paper 2002-2744, June 2002.

[2]Berry, S. A., Horvath, T. J., Hollis, B. R., Thompson, R. A., Hamilton II, H. H., "X-33 Hypersonic Boundary Layer Transition," *Journal of Spacecraft and Rockets*, Vol. 38, No. 5, pp. 646-657, Sept.-Oct. 2001.

[3]Hollis, B.R. and Liechty, D.S., "Boundary Layer Transition Correlations and Aeroheating Predictions

for Mars Smart Lander," AIAA Paper 2002-2745, June 2002.

[4]Crusciel, G. T., "Active and Passive Boundary Layer Tripping," AIAA 97-2016, June 1997.

[5]Bouslog, S. A., An, M. Y., Campbell, C. H., Wang, K. C., and Pelley, R. L., "Orbiter Boundary-Layer Transition Working Group: Analysis and Ground Test Status Report," NASA Johnson Space Center, JSC-26812, Oct. 1994.

[6]Freeman Jr., D. C., Talay, T. A., and Austin, R. E., "Reusable Launch Vehicle Technology Program," AIAA Paper IAF 96-V.4.01, Oct. 1996.

[7]Powell, R. W., Lockwood, M. K., and Cook, S. A., "The Road from the NASA Access-to-Space Study to a Reusable Launch Vehicle," AIAA Paper IAF 98-V.4.02, Sept. 1998.

[8]Baumgartner, R.I., and Elvin, J. D., "Lifting Body - An Innovative RLV Concept," AIAA Paper 95-3531, Sept. 1995.

[9]Thompson, R.A., Hamilton II, H. H., Berry, S. A., and Horvath, T. J., "Hypersonic Boundary Layer Transition for X-33 Phase II Vehicle," AIAA Paper 98-0867, Jan. 1998.

[10]Hamilton II, H. H., Weilmuenster, K. J., Berry, S. A., and Horvath, T. J., "Computational/Experimental Aeroheating Predictions for X-33 Phase II Vehicle," AIAA Paper 98-0869, Jan. 1998.

[11]Berry, S. A., Horvath, T. J., Kowalkowski, M. K., and Liechty, D. S., "X-33 (Rev-F) Aeroheating Results of Test 6770 in NASA Langley 20-Inch Mach 6 Air Tunnel," NASA TM-1999-209122, March 1999.

[12]Hollis, B. R., Horvath, T. J., Berry, S. A., Hamilton II, H. H., Thompson, R. A., and Alter, S. J., "X-33 Computational Aeroheating Predictions and Comparison with Experimental Data," *Journal of Spacecraft and Rockets*, Vol. 38, No. 5, pp. 658-669, Sept.-Oct. 2001.

[13]Horvath, T. J., Berry, S. A., Hollis, B. R., Liechty, D. S., Hamilton II, H. H., and Merski, N. R., "X-33 Experimental Aeroheating at Mach 6 Using Phosphor Thermography," *Journal of Spacecraft and Rockets*, Vol. 38, No. 5, pp. 634-645, Sept.-Oct. 2001.

[14]Thompson, R. A., "Review of X-33 Hypersonic Aerodynamic and Aerothermodynamic Development," 22nd International Congress of the Aeronautical Sciences, ICA-0323, Aug. 27 - Sept. 1, 2000.

[15]Palmer, G., Kontinos, D., and Sherman, B., "Surface Heating Effects of X-33 Vehicle TPS Bowing, Steps, and Gaps," AIAA Paper 98-0865, Jan. 1998.

[16]Prabhu, D. K., Wright, M. J., Marvin, J. G., Brown, J. L., and Venkatapathy, E., "X-33 Aerothermal Design Environment Predictions: Verification and Validation," AIAA Paper 200-2686, June 2000.

[17]Prabhu, D. K., Loomis, M. P., Venkatapathy, E., Polsky, S., Papadopoulos, P., Davies, C. B., and Henline, W.D., "X-33 Aerothermal Environment Simulations and Aerothermodynamic Design," AIAA Paper 98-0868, Jan. 1998.

[18]Berry, S. A., Bouslog, S. A., Brauckmann, G. J., and Caram, J. M., "Boundary Layer Transition due to Isolated Roughness: Shuttle Results from the LaRC 20-Inch Mach 6 Tunnel," AIAA Paper 97-0273, Jan. 1997.

[19]Horvath, T. J., Berry, S. A., Merski, N. R., Fitzgerald, S. M., "X-38 Experimental Aerothermodynamics," AIAA Paper 2000-2685, June 2000.

[20]Hollis, B. R., "Real-Gas Flow Properties for NASA Langley Research Center Aerothermodynamic Facilities Complex Wind Tunnels," NASA CR 4755, Sept. 1996.

[21]Buck, G.M., "Automated Thermal Mapping Techniques Using Chromatic Image Analysis," NASA TM 101554, April 1989.

[22]Buck, G.M., "Surface Temperature/Heat Transfer Measurement Using a Quantitative Phosphor Thermography System," AIAA Paper 91-0064, January 1991.

[23]Merski, N.R., "A Relative-Intensity, Two-Color Phosphor Thermography System," NASA TM 104123, September 1991.

[24]Merski, N.R., "Reduction and Analysis of Phosphor Thermography Data with the IHEAT Software Package," AIAA Paper 98-0712, January 1998.

[25]Buck, G.M., and Vasques, P., "An Investment Ceramic Slip-Casting Technique for Net-Form, Precision, Detailed Casting of Ceramic Models," U.S. Patent 5,266,252, November 1993.

[26]Fay, J.A., and Riddell, F.R., "Theory of Stagnation Point Heat Transfer in Dissociated Air," *Journal of Aeronautical Sciences*, Vol 25, No. 2, 1958, pp. 73-85.

[27]Hamilton II, H. H., Greene, F. A., DeJarnette, F. R., "Approximate Method for Calculating Heating Rates on Three-Dimensional Vehicles," *Journal of Spacecraft and Rockets*, Vol. 31, No. 3, pp. 345-354, 1994.

[28]Gnoffo, P.A., "An Upwind-Biased, Point-Implicit Algorithm for Viscous, Compressible Perfect-Gas Flows," NASA TP-2953, February 1990.

[29]Cheatwood, F.M., Gnoffo, P.A., "User's Manual for the Langley Aerothermodynamic Upwind Relaxation Algorithm (LAURA)," NASA TM-4674, April 1996.

[30]Roe, P. L., "Approximate Riemann Solvers, Parameter Vectors and Difference Schemes," *Journal of Computational Physics*, Vol. 43, No. 2, pp. 357-372, 1981.

[31]Harten, A., "High Resolution Schemes for Hyperbolic Conservation Laws," *Journal of Computational Physics*, Vol. 49, No. 3, pp. 357-393, 1983.

[32]Yee, H. C., "On Symmetric and Upwind TVD Schemes," NASA TM 88325, 1990.

[33]"GASP Version 3, The General Aerodynamic Simulation Program, Computational Flow Analysis Software for the Scientist and Engineer, User's Manual," AeroSoft, Inc., Blacksburg, VA, May 1996.

[34]Zoby, E. V., Moss, J. N., and Sutton, K., "Approximate Convective-Heating Equations for Hypersonic Flows," *Journal of Spacecraft and Rockets*, Vol. 18, No. 1, 1981, pp. 64-70.